Polymer Chemistry

ARTICLE

Well-defined hyperstar copolymers based on a thiol-yne hyperbranched core and a poly(2-oxazoline) shell for biomedical applications

Received 00th January 20xx,
Accepted 00th January 20xx

DOI: 10.1039/x0xx00000x

www.rsc.org/

Matthias Hartlieb,[a] Thomas Floyd,[a] Alexander B. Cook,[a] Carlos Sanchez-Cano,[a] Sylvain Catrouillet,[a,†] James Burns,[c] Sébastien Perrier[a, b, *]

Well defined 'hyperstar' copolymers were synthesized by combining hyperbranched polymers produced by thiol-yne chemistry with poly(oxazoline)s. The hyperbranched core was prepared using an AB_2 monomer and a trifunctional alkene, applying a monomer feeding approach. The degree of branching was high (0.9) while maintaining low dispersities (1.3). Poly(2-ethyl-2-oxazoline) (PEtOx) functionalized by a thiol end group was coupled to the surface of the hyperbranched structure accessing terminal alkyne units. PEtOx-SH was produced by termination of the living polymerization with ethyl xanthate and subsequent conversion to thiol under alkaline conditions. The degree of polymerization was varied producing PEtOx with 23 or 42 repeating units, respectively with a dispersity around 1.1. After conjugation of the polymer arms, hyperstar copolymers were characterized by SEC, NMR spectroscopy, light scattering, and AFM. The polymers were able to encapsulate the hydrophobic dye nile red within the core of the structure with loading efficiencies between 0.3 and 0.9 wt%. Cytotoxicity of the hyperstars was assessed using A2780 human ovarian carcinoma cells resulting in IC_{50} values around 0.7 mg ml^{-1}. Successful internalization and colocalization with lysosomal compartments was observed by confocal microscopy studies.

Introduction

The use of polymer based drug delivery systems has received increasing interest in the last decades.[1] Beside nanoparticels[2] most prominently, polymeric micelles, composed of amphiphilic diblock copolymers have been extensively used to deliver payloads.[3] These polymers are able to phase segregate in aqueous solution forming hydrophobic compartments protected by a hydrophilic shell. Drug molecules can be encapsulated within the core of the micelle and released upon delivery to the intended target tissues, by passive (EPR effect)[4] or active targeting methods.[5] However, micelles suffer from their dynamic nature; they disassemble below the critical micelle concentration, which can lead to the premature release of their payload upon administration.[6] This issue can be addressed by the use of unimolecular micelles, such as dendrimers possessing a hydrophilic shell,[7] as they are not able to disassemble even at high dilutions. However, the synthesis and upscaling of these materials is highly demanding when compared to polymeric micelles.

Hyperbranched polymers are a promising alternative for dendrimers, as they offer high degrees of branching (DB, usually ranging between 0.4 and 0.6) while being able to be produced by relatively simple and scalable synthetic approaches.[8] Higher DB values can be achieved using AB_2 or AB_3 monomers, multifunctional core molecules, and efficient polymerization reactions such as esterification[9] or more recently radical thiol-yne addition[10] and copper mediated azide-alkyne cycloadditions (CuAAc).[11, 12]

A major drawback of hyperbranched polymers is their relatively high dispersity ($Đ$ > 3.0).[13] By using thiol-yne chemistry and a monomer feeding approach our group has recently developed a method to produce hyperbranched polymers with very high degrees of branching (DB > 0.8) while maintaining low dispersities ($Đ$ < 1.3).[14] However, in order to improve the application of these architectures as a drug delivery vehicle, a hydrophilic shell can be added.[15] As the surface of hyperbranched polymers is densely populated with functional groups, end functionalized polymers can be coupled to the dendritic polymer, resulting in hyperstar copolymers.

Poly(2-oxazoline)s (POx) are a promising polymer class for the synthesis of hyperstar copolymers. Small side chain derivatives such as poly(2-methyl-oxazoline) or poly(2-ethyl-oxazoline) (EtOx) are generally regarded as biocompatible[16-18] and show a stealth effect comparable to poly(ethylene glycol).[19-21] PEtOx even shows higher circulation times and lower unspecific accumulation in the body compared to PEG.[22] POx can be produced by cationic ring opening polymerization (CROP) of oxazolines offering a multitude of potential functionalities.[23, 24]

a Department of Chemistry, The University of Warwick, Coventry CV4 7AL, UK;
b Faculty of Pharmacy and Pharmaceutical Sciences, Monash University, 381 Royal Parade, Parkville, Victoria 3052, Australia
c Syngenta, Jealott's Hill International Research Centre, Bracknell, Berkshire, RG42 6EY, United Kingdom
† - Current address: Institut Charles Gerhardt Montpellier UMR5253 CNRS-UM-ENSCM, Université de Montpellier, F-34095, Montpellier Cedex 5, France

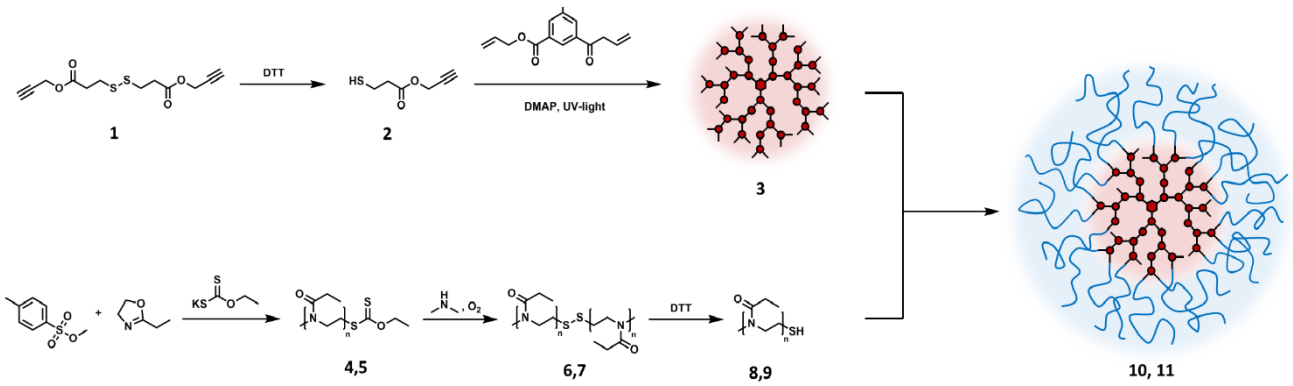

Scheme 1: Schematic representation of the synthesis of thiol-yne and POx based hyperstar copolymers.

The beneficial properties of POx based surface coatings,[25] micelles[26, 27] star shaped copolymers,[28] as well as microgels,[21, 29] nanogels[30-32] or capsules[33-35] in a biomedical context have been demonstrated in multiple reports.

The combination of dendrimers and hyperbranched polymers decorated with POx arms has previously been described in literature.[36] Generally, such hyperstars can be synthesized in a core-first approach, where the multiple functionalities of the surface of the branched structure are used as an initiator for the CROP. This was demonstrated by the use of hyperbranched polymer based on poly(glycidol),[37] poly vinyl benzyl chloride,[38] or hydroxyphenyl valeric acid.[39] Alternatively, linear polymer chains can be attached in an arm-first approach as shown for glycogen,[40] poly(propylene imine) dendrimers,[41] or poly(urea) dendrimers[42] by an end capping of the living CROP. Furthermore, POx with functionalities reactive towards amines were used to decorate branched poly(ethylene imine),[43] poly(amidoamine),[44] and lysine dendrimers.[45] Recently, it was shown that POx-based hyperstars show great promise in vivo in the treatment of cancer.[46]

In this article, we describe the combination of the beneficial properties of POx with narrow dispersity and high DB of thiol-yne based hyperbranched polymers as an easy way to hyperstar copolymers (**Scheme 1**). Thiol end functionalized POx was produced using a two-step procedure involving end capping of the living polymerization with ethyl xanthate and subsequent aminolysis. Although functionalization of POx with thiol end groups has been described previously using termination with NaSH[47] or thioacetate,[48, 49] and functionalization by CuAAc,[29] the end capping of a living CROP with a xanthate[50] followed by aminolysis[51] offeres a novel and efficeint route to thiol functionalized polymers. Synthesized hyperstars were characterized *via* light scattering and atomic force microscopy techniques. The potential as drug delivery vectors of the resulting unimolecular nanoparticles was illustrated by loading them with the hydrophobic nile red, used as a drug model. The resulting materials were found to have moderate cytotoxicity and cell internalisation studies revealed an endocytosis pathway, resulting in colocalization with lysosomal compartments. In contrast to previously described hyperstar systems, the herein presented polymer does not require tedious dendrimer synthesis while the product is still well defined.

Results and Discussion

Hyperbranched Polymers by thiol-yne chemistry

The thiol-yne monomer, prop-2-yn-1-yl 3-mercaptopropanoate (PYMP), used to produce the hyperbranched core of the hyperstar copolymers was synthesized according to literature procedure.[14] Briefly, 3,3-dithiodipropionic acid was activated using N-(3-Dimethylaminopropyl)-N'-ethylcarbodiimide (EDC) and 4-Dimethylaminopyridine (DMAP). Propargyl alcohol was added to the solution to yield the protected form of the monomer, di(prop-2-yn-1-yl) 3,3'-disulfanediyldipropionate (**1**). Deprotection was accomplished under reductive conditions using dithiothreitol (DTT), yielding the thiol-yne bearing PYMP monomer (**2**). Both, precursor and monomer were characterized using NMR spectroscopy (**Figure S1**).

The synthesis of hyperbranched copolymers using PYMP was previously optimized in our group to yield systems with a high degree of branching, as well as low dispersities.[14] Key factors are the use of an alkene core (triallyl 1,3,5-Benzenetricarboxylic acid) and a low monomer concentration accomplished by a feeding approach. In the presence of a photo initiator, 2,2-dimethoxy-2-phenylacetophenone (DMPA), and a source of UV light, a polymer with high degree of branching (0.9) and a low dispersitiy (1.29) was synthesised. The degree of branching was determined by ^{1}H-NMR spectroscopy comparing the signals of branched, terminal and linear units (**Figure S2**).

Size exclusion chromatography (SEC) measurements in DMF showed a mono-modal distribution for refractive index and light scattering detectors indicating the absence of cross linking (**Figure S3**). A PMMA calibration was used to determine the molar mass of the polymer (M_n = 6,000 g mol^{-1}). Due to the globular structure of the hyperbranched polymer, a significant difference in the hydrodynamic volume compared to the linear standard used to calibrate the measurements was expected. However, the measurement illustrates the absence of coupling reactions during the polymerization.

To determine the absolute molar mass of poly(PYMP) (**3**), static light scattering (SLS) in DMF was employed (**Figure S4**).

Table 1: Characterization data of PEtOx with varying DP values after end functionalization using ethyl xanthate and after aminolysis and oxidation.

Sample	Composition	DP[a]	Conv.[a] (%)	DF (%)[a,b]	$M_{n,\,NMR}$[a] (g mol^{-1})	$M_{n,\,SEC}$[c] (g mol^{-1})	$Đ$[c]
4	$PEtOx_{23}$-Xan	23	97	88	2,400	3,200	1.09
5	$PEtOx_{42}$-Xan	42	94	89	4,300	5,900	1.12
6	$PEtOx_{23}$-S-S-$PEtOx_{23}$	-	-	-	4,800	4,900	1.10
7	$PEtOx_{42}$-S-S-$PEtOx_{42}$	-	-	-	8,600	11,700	1.11

a) Determined from ^{1}H NMR spectroscopy. b) DF = Degree of Functionalization. c) Determined by SEC in DMF using a DRI detector and PMMA standard.

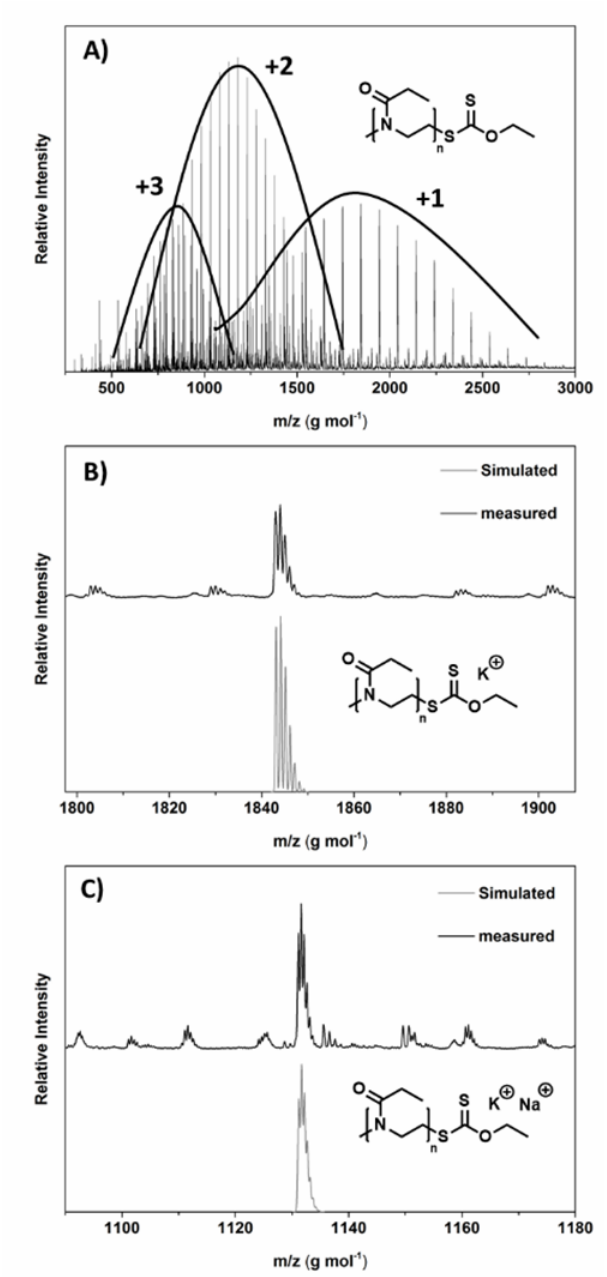

Figure 1: A) ESI-mass spectrum of $PEtOx_{23}$ terminated with ethyl xanthate (**4**). B) Overlay of simulated and measured isotopic pattern for single charged species. C) Overlay of simulated and measured isotopic pattern for double charged species.

Using the refractive index increment, dn/dC also determined in DMF (dn/dC = 0.102), a molar mass of 11,500 g mol^{-1} was determined. The difference between the values obtained by SLS and SEC illustrate the branched nature of synthesized polymer.

After purification, the polymer was found to cross-link and gelate within days when stored in bulk, potentially due to the presence of residual photo initiator causing alkyne-alkyne coupling. This hampered the preparation of large batches of the material for PEtOx conjugation. The issue was addressed by removing residual photo initiator by precipitation, and storing the polymer in solution (DMF, 20 mg mL^{-1}) at -20˚C. The polymer proved to be stable for at least one month when stored under these conditions (**Figure S5**).

Thiol end functionalized Poly(2-oxazoline)s

In order to produce PEtOx able to be coupled to the surface of poly(PYMP), the POx had to be funcionalised with a thiol end group. To ensure quantitative end functionalization and a defined degree of polymerization (DP) the kinetics of the polymerization had to be investigated. Knowledge about the rate constant enables the prediction of conversion for a specific polymerization. The polymerization of EtOx was carried out in a schlenk-flask in acetonitrile under nitrogen atmosphere at 78°C, aiming for a DP of 50. Both, initiator and monomer were distilled to dryness prior to use. During the polymerization, samples were taken at specific time points to analyse conversion, molar mass and dispersity. The conversion was determined by NMR spectroscopy comparing the signals of the oxazoline ring and the polymer backbone. Molar mass distribution was determined by SEC using chloroform as an eluent and poly(styrene) as a calibration standard. The evolution of $\ln(M_0/M_t)$ over time and the increase of molar mass as a function of the conversion were found to be linear indicating a living polymerization process (**Figure S6**). A rate constant of 5.6×10^{-3} L mol^{-1} was obtained.

The functionalization of PEtOx with thiols was achieved via the termination of the living polymerization process using potassium ethyl xanthate, which was used as a precursor for the aimed functionality (Scheme 1). After addition of the salt to the polymerization mixture under a nitrogen atmosphere, immediate precipitation of potassium tosylate was observed indicating a successful end functionalization.

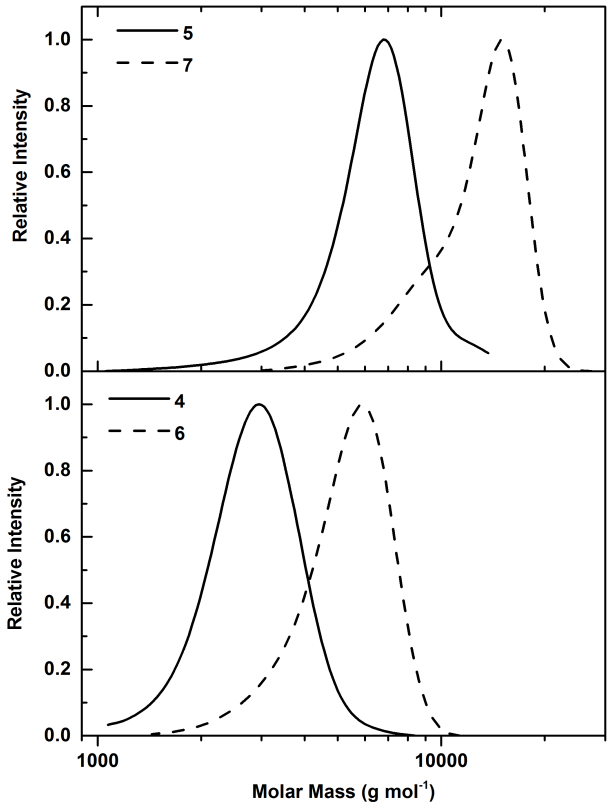

Figure 2: SEC traces of PEtOx-Xanthate (**4**, **5**) as well as polymers after aminolysis and oxidative coupling (**6**, **7**). PMMA was used as a calibration standard for the measurements.

In order to study the influence of the chain length on the solubilisation of hyperstars in water and their performance as drug delivery vehicles, two different PEtOx-xanthate polymers targeting a DP of 25 and 50 were produced (**4**, **5**). A conversion of 95% was targeted in order to avoid side reactions prior to end capping and, at the same time, reach the desired DP. The conversion was determined by NMR spectroscopy before end capping by comparing the signals of the backbone with the signals of residual EtOx.

The DP, as well as the degree of functionalization (DF) with ethyl xanthate was determined via NMR spectroscopy after precipitation, by comparison of the signal of the polymer backbone with the peak of the methyl group at the α-chain end or with the methyl group of the xanthate, respectively (**Figure S7**). The obtained DP values (23 and 42) were lower than the targeted values (24 and 47.5), due to incomplete monomer conversion and experimental error in the analysis. The DF was found to be higher than 85% for both polymers (**Table 1**).

To prove the insertion of the desired end group, ESI mass spectrometry of polymers with DP 25 was performed (**Figure 1**). Two main distributions were observed, corresponding to the

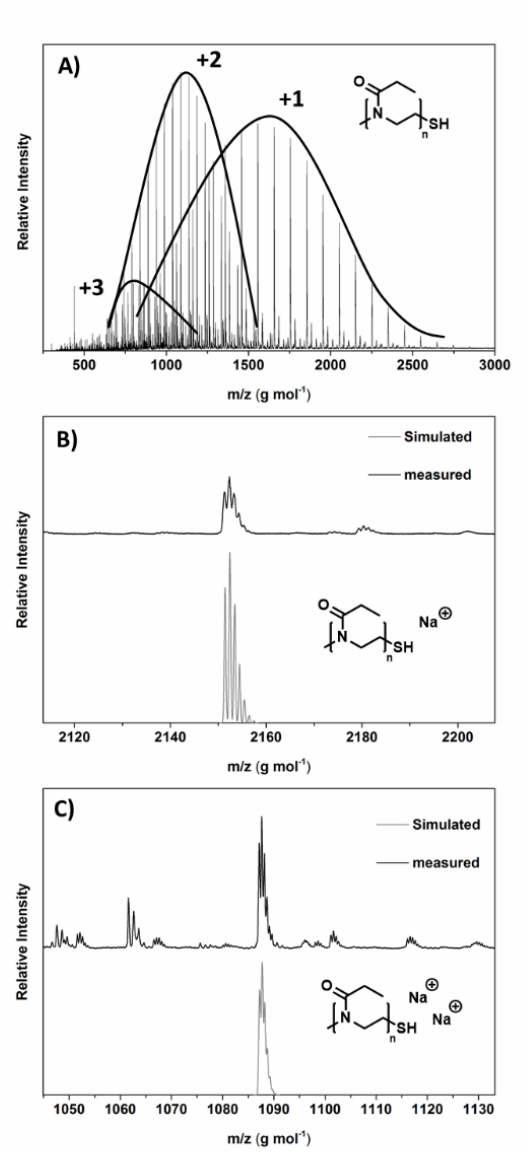

Figure 3: A) ESI-mass spectrometry of $PEtOx_{23}$ after aminolysis (**8**). B) Overlay of simulated and measured isotopic pattern for single charged. C) Overlay of simulated and measured isotopic pattern for double charged species.

desired species with one or two charges, respectively. The overlay of the measured spectrum with simulated isotopic pattern proved the existence of polymers initiated by a methyl group and having a xanthate group at the ω-chain end. Smaller distributions in the enhanced region correspond to species with different counter ions and/or state of charge.

The molar mass, determined by SEC measurements was in the expected range, although a PMMA calibration was used (**Table 1**). Obtained dispersities were low, indicating a living polymerization process.

The xanthate group was converted into a thiol *via* aminolysis using dimethylamine in ethanol at 40°C for 3h. The reaction resulted in the formation of a thiourethane and a thiol end functionalized polymer chain. The formed PEtOx-SH were found to be susceptible to oxidation at ambient conditions.

Table 2: Characterization of hyperbranched polymer and hyperstar copolymers.

Sample	SLS in DMF			SLS in water			SEC		NMR		Nile red loading	
	M_a[a] (g mol^{-1})	N_{agg}[b]	R_h (nm)	M_a[a] (g mol^{-1})	N_{agg}[b]	R_h (nm)	Mn	Đ	Arms	Mn	wt%	mol%
3	11,500	-	8	-	-	-	6,000	1.29	-	-	-	-
10	254,000	3.7	41	311,000	4.5	6	13,800	1.30	24	69,000	0.9	2
11	259,000	2.4	45	445,000	4.1	8	24,200	1.28	23	110,400	0.3	0.7

[a] Apparent molecular weight determined by the SLS. [b] Determined by comparison of M_a (SLS) and M_n (NMR).

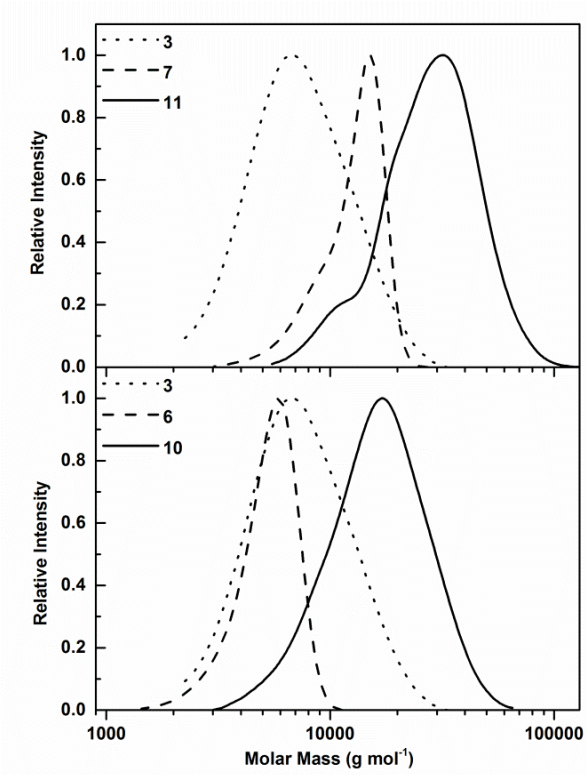

Figure 4: SEC measurements of poly(PYMP) (**3**), PEtOx (**6**, **7**) and hyperstar copolymers (**10**, **11**) in DMF using a PS calibration standard.

SEC measurements after purification showed increased molar mass values as compared to the precursor polymer. This was attributed to oxidative chain coupling during the extraction process, which was supported by the doubled molar mass of PEtOx as indicated by SEC measurements. The mono-modal distribution and low dispersities suggest a near quantitative thiol functionalization of PEtOx (**Figure 2**). For $PEtOx_{42}$, a small tail at low molecular weight indicates the presence of either unfunctionalized or non-oxidized chains. As the control over the polymerization decreases with increasing monomer initiator ratios, this behaviour was expected. Nevertheless, the majority of chains were thiol end-functionalized for both DPs. NMR spectra clearly showed the disappearance of signals attributed to ethyl xanthate, supporting a quantitative aminolysis (**Figure S7**).

To enable thiol-yne based coupling between the hyperbranched polymer and PEtOx chains, oxidized polymers were reduced using DTT in dichloromethane. The reducing agent was removed *via* extraction with water under oxygen free conditions, and the resulting polymers were analysed *via* ESI mass spectrometry (**Figure 3**). Again, one single and one double charged main distribution were observed, both attributed to thiol end functionalized PEtOx. Smaller distributions in the enhanced region correspond to species with different counter ions and/or state of charge

Synthesis and characterization of hyperstar copolymers

The conjugation of PEtOx and poly(PYMP) was performed in DMF using DMPA under UV light as a radical source. The reaction was performed under nitrogen atmosphere to prevent oxidation of PEtOx-SH and the consumption of radicals by oxygen.

The number of alkyne functionalities for an individual core was determined by NMR spectroscopy and SLS. The M_a of the hyperbranched core was found to be 11,500 g mol^{-1} by light scattering. Subtracting the weight of the tri-allyl core (10%) results in a DP of 72 including terminal, linear and branched units. As 44 % of the monomer units were terminal, as determined by NMR, the total number of alkyne functionalities per poly(PYMP) is 32. For coupling reactions, a 1:1 ratio of PEtOx to alkyne functionality was used. This value should result in a sufficient surface coverage of hyperstar copolymer to ensure water solubility. Remaining alkyne or alkene functions can potentially be used for further functionalization reactions. The reaction mixture was diluted with water and filtered to remove any insufficiently reacted poly(PYMP). Residual PEtOx was removed by dialysis using centrifuge filter tubes using a membrane with a 10 kDa cut off.

The obtained hyperstar copolymers were analysed using SEC in DMF (**Figure 4**, **Table 2**). The dispersities were found to be similar to the hyperbranched starting material while the molar mass increased significantly. A higher molar mass was obtained when using PEtOx with a DP of 42 as compared to DP 23. This indicates that a similar number of polymer arms were attached in each case. The low molecular weight shoulder of polymer **11** could be attributed to residual linear polymer which was not removed quantitatively be dialysis.

NMR spectroscopy was used to analyse the ratio between poly(PYMP) and PEtOx by comparison of the monomer methylene signals at 4.23 and 3.82 ppm with the signals of the PEtOx polymer backbone at 3.46 ppm (**Figure S8**).

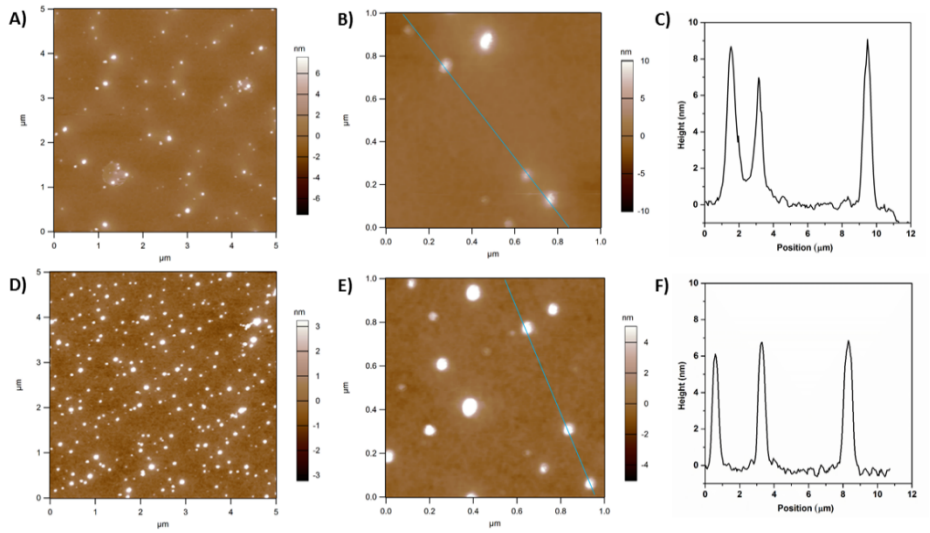

Figure 5: AFM images of hyperstars drop-casted from a solution of 0.1 mg mL^{-1} hyperstar in THF. A) Compound **10**, 5 µm scan size, B) Compound **10**, 1 µm scan size, C) Height profile of compound **10**, D) Compound **11**, 5 µm scan size, E) Compound **11**, 1 µm scan size, F) Height profile of compound **11**.

As the DP value is known for both initial polymers, the number of arms per hyperstar could be calculated. Both hyperstars have a similar number of arms (24 arms for compound **10** and 23 arms for compound **11**), which are both lower than the targeted value of 32. This can be explained by an incomplete conversion of the thiol-yne reaction, possibly caused by steric hindrance or by the presence of unfunctionalized PEtOx. In fact, some of the alkyne functionalities might be located on the inside of the hyperbranched structure, inaccessible for polymer chains. The molar mass of the conjugates calculated from these values was 69,000 and 110,000 g mol^{-1}, markedly higher than the molar mass obtained by SEC, which can be explained by the hyperbranched nature of the polymer and the lack of a hyperbranched SEC standard.

Static light scattering was employed to determine the absolute molar mass of the synthesized hyperstar copolymers. In order to minimize possible aggregation, measurements were first performed in DMF, as poly(PYMP), as well as PEtOx are soluble in this solvent. Both hyperstar polymers were analysed at concentrations between 10 and 0.5 mg mL^{-1} (**Figure S9** and **S10**). The results as displayed in **Table 2** showed a significant difference compared to the values obtained by NMR spectroscopy. Both hyperstars were found to have a molar mass around 250,000 g mol^{-1}. In the case of PEtOx$_{23}$, this value would correspond to a number of arms above 100, which is higher than the available number of conjugation sites per poly(PYMP). In the case of PEtOx$_{42}$, quantitative conversion of the all alkyne functionalities would be required to reach such a molecular weight. Therefore, the values are likely to be the result of aggregation of multiple hyperstars. This is supported by the hydrodynamic radius of 40 nm, which is larger than expected for non-aggregated hyperstars. Taking the molar mass calculated from NMR as a basis, a number of aggregation (N_{agg}) of 4 and 2, respectively, were calculated.

A possible explanation for this behaviour can be found in the purification protocol (dialysis in aqueous medium) of the hyperstar copolymers. Since the conjugation was performed in a 1:1 stoichiometry of alkyne and thiol, and given the resulting vinyl thiolether has an increased reactivity towards thiols as compared to the alkyne moieties, a reaction of two polymers per site is possible despite steric hindrance. This could lead to the presence of hydrophobic patches on the surface of the hyperbranched structure, leading to a self-assembly in aqueous solution due to the hydrophobic effect and a possible entanglement, which persists even after re-solubilisation in DMF. This assumption is supported by a higher number of aggregation for compound **10**, which has shorter PEtOx arms, compared to compound **11**. This steric stabilization is less pronounced leading to a higher tendency to aggregate. The mono-modal size distribution in SEC can be explained by the high shear forces on the column, breaking apart the assembled structures.

SLS in water was performed to elucidate the molecular weight of the system in a polar solvent (**Figure S11** and **S12**). Molecular weight, as well as N_{agg} were found to increase as compared to measurements in DMF indicating an increased tendency of assemble in water. Furthermore, the hydrodynamic radius is drastically decreased in water, which could be attributed to a collapse of the hydrophobic core, while in DMF poly(PYMP) swells leading to an increased radius. DLS measurements of the hyperstars (**Figure S13**) show a small portion of large aggregates (around 50 nm) for sample **10** whereas only one sharp distribution is detected for hyperstar **11**. This is in accordance with an increased shielding ability of DP 50 PEtOx compared to the shorter polymer. It is important to emphasise that in both cases assembled structures are well defined nano-aggregates shielded by a PEtOx shell.

To illustrate size and size distribution, atomic-force microscopy (AFM) was utilized to image hyperstar copolymers (**Figure 5**). Samples were dissolved in THF, which is expected to solubilize both, core and shell, and drop casted onto silicon. After drying, the height profile was measured using tapping mode. For both

polymers the profile shows a height between 6 and 8 nm, which is consistent with the expectations for a soft hyperstar structure deposited on a surface.

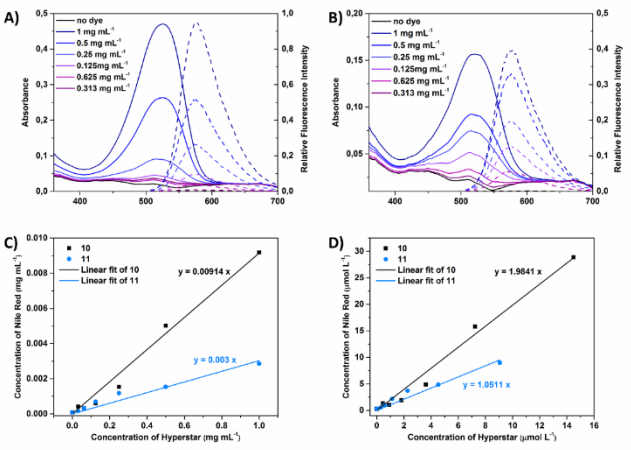

Figure 6: Nile red loading of hyperstar copolymers. A) Absorbance (solid) and fluorescence (dashed) spectra of Nile red solubilized by varying concentrations of hyperstar **10**. B) Absorbance (solid) and fluorescence (dashed) spectra of Nile red solubilized by varying concentrations of hyperstar **11**. C and D) Determination of nile red loading per hyperstar by weight (C) or molar (D) concentration using the absorbance at 520 nm.

From the size of the imaged structures, ranging between 20 and 50 nm, minor aggregation of few hyperstar molecules as a result of the drying process can be concluded.

Dye loading of hyperstar copolymers

The ability of the hyperstar copolymers to encapsulate hydrophobic molecules was investigated using nile red, a fluorophore typically used as a model drug of intermediate lipophilicity (log P ~ 3–5) such as the potent chemotherapeutic Paclitaxel. As hyperstars are essentially unimolecular micelles the loading process could be conducted in THF, which solubilizes both fluorophore and hyperstar. To study the loading capacity of hyperstars varying amounts of polymer were added to a constant amount of nile red. By slow evaporation of the solvent, nile red was forced into the hydrophobic domains (poly(PYMP)). Subsequently, water was added to dissolve the fluorophore loaded hyperstars. As the PEtOx decorated polymers are, in contrast to nile red, readily water soluble, non-encapsulated nile red could be separated by filtration.

To determine the exact amount of loaded dye, samples were freeze dried to remove the water and re-dissolved in THF. This was necessary to exclude solvato-chromic effects altering the absorption and emission profile as a result of the environment within the hyperbranched core. To determine the amount of encapsulated nile red, absorbance intensities were used and compared to a calibration of fluorophore alone in THF (**Figure S14**). The absorbance at 520 nm was recorded in dependence of the concentration of hyperstar polymer, able to solubilize the dye (**Figure 6A** and **B**).

By plotting the weight concentration of nile red versus the weight concentration of hyperstar a loading capacity can be determined using the slope of the linear fit (**Figure 6C**). Loading capacities of 0.9 and 0.3 wt% were obtained for hyperstars **10** and **11**, respectively. As the content of PEtOx in polymer **11** is higher as compared to polymer **10** a lower amount of encapsulated dye (in wt%) was expected as also the percentage of hydrophobic compartment per hyperstar is decreased.

Based on the molecular weight determined by NMR spectroscopy and SLS a molar loading capacity was calculated (2 mol% for polymer 10 and 0.7 mol% for polymer 11), which is in perfect agreement with reports on other nile red loaded hyperstar copolymers.[52-54] Both hyperstars copolymers show a similar loading efficiency, which was expected as the hydrophobic compartment is identical.

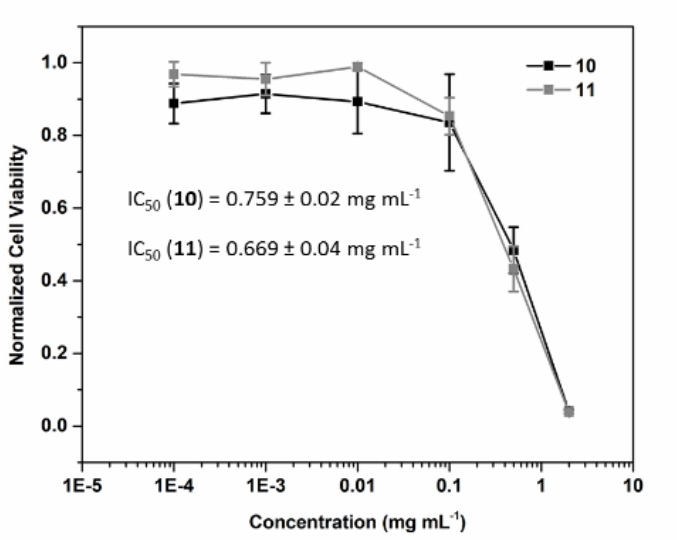

Figure 7: Cell viability of A2780 human ovarian carcinoma cells treated with hyperstars **10** and **11** for 72 h at 37°C.

Biological behaviour of hyperstar copolymers

Synthetic polymer systems have to meet a number of key requirements to be used as drug carrier. Most importantly, the delivery vector should show no or a low cytotoxicity against mammalian cells. The ability of the hyperstar copolymers to inhibit the cell growth of A2780 human ovarian carcinoma cells was tested using the SRB assay, and IC_{50} values obtained for **10** and **11** were above 0.5 mg mL^{-1} (**Figure 7**), which is higher than concentrations relevant for drug delivery applications. The ability of both hyperstar molecules to inhibit cell growth at concentrations above 0.5 mg mL^{-1}, could be attributed to incomplete coverage of the hydrophobic surface of the hyperbranched polymer by the PEtOx. Exposed hydrophobic domains could potentially interact with cellular membranes or interfere with processes within the cell. Surprisingly, both hyperstar copolymers inhibit the cell growth of A2780 similarly, whereas the ratio of biocompatible PEtOx is slightly higher for compound **11**.

Additionally, confocal microscopy was used to assess the cellular uptake of dye loaded hyperstar copolymers. A2780 cells were incubated for two hours with non-inhibiting concentrations (0.1 mg/mL^{-1}) of **10** and **11**. Nile red fluorescence within the cell showed that the hyperstars are taken up readily by cells (**Figure S15**). Fluorescence microscopy

with different organelles staining agents was used to evaluate cellular localization.

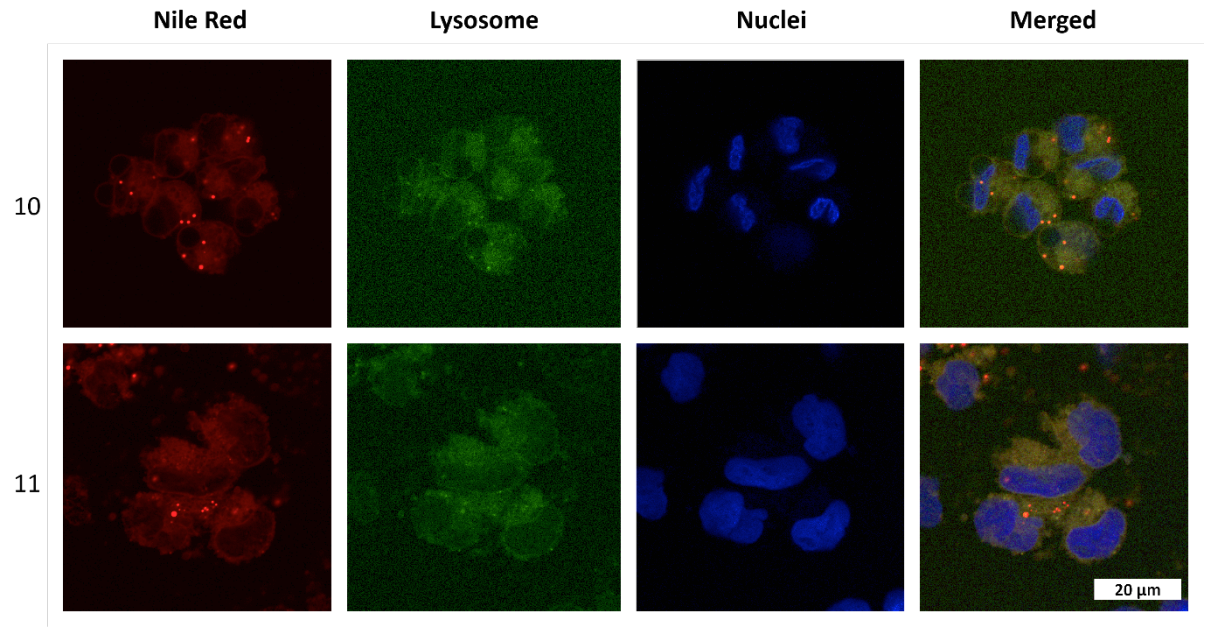

Figure 8: Confocal images of A2780 human ovarian carcinoma cells treated with nile red loaded hyperstars (**10**, **11**) for 2 h at 37˚C at a concentration of 0.1 mg mL^{-1}. Lysosomal compartments were stained using LysoTracker® green DND-26, nuclei were stained using Hoechst 33258.

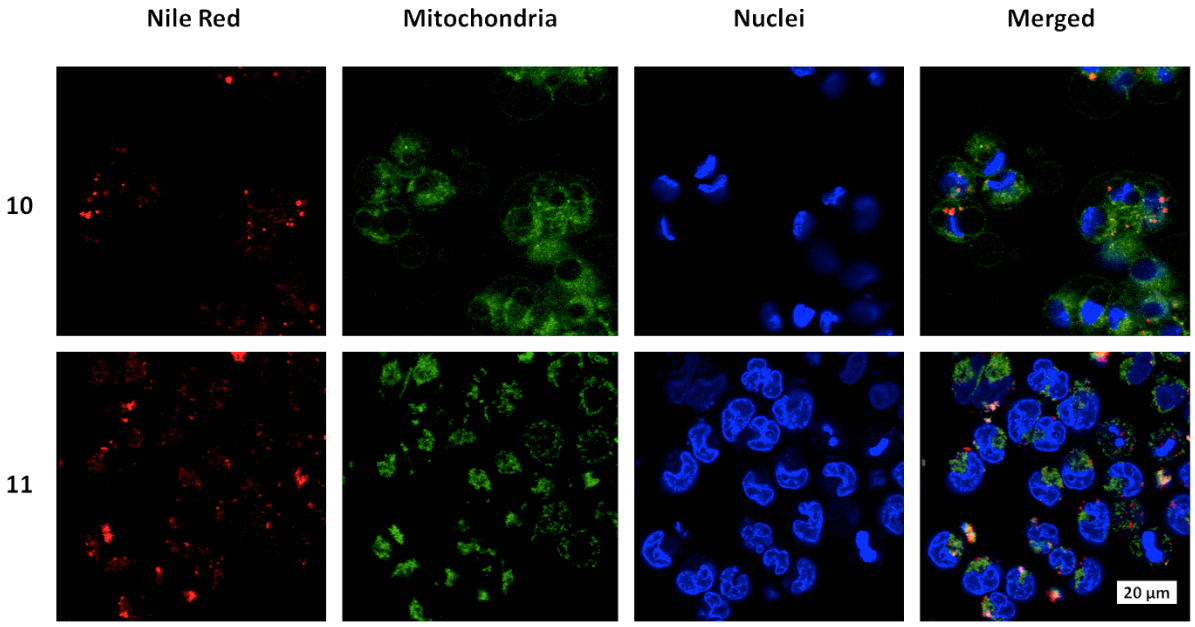

Figure 9: Confocal images of A2780 human ovarian carcinoma cells treated with nile red loaded hyperstars (**10**, **11**) for 2 h at 37˚C at a concentration of 0.1 mg mL^{-1}. Mitochondria were stained using MitoTracker® green FM, nuclei were stained using Hoechst 33258.

Nuclei were stained using Hoechst 33258, and either lysosomes or mitochondria were labelled with LysoTracker® Green (**Figure 8**) or MitoTracker® Green (**Figure 9**), respectively.

These experiments clearly show that hyperstars are able to pass through the cellular membrane, but do not reach the nucleus, being concentrated in the cytoplasm of the cell. When their localization is compared with lysosomal staining, a strong colocalization of green and red fluorescence was observed. On the contrary, MitoTracker® and nile red was not found in the same cellular areas. These results suggest an accumulation in the lysosomal compartments and not in the mitochondria of

treated cells, and indicates an energy dependent uptake mechanism (e.g. endocytosis), which was expected from a polymer of this size.

Nevertheless, although the dye is not covalently coupled to the hyperstars, not allowing to make any conclusive statement about the fate of **10** and **11**, both hyperstar systems are not expected to degrade under physiological conditions within a relevant time frame . The monomer units of the hyperbranched core contain ester bonds, but the hydrophobic nature of the structure should prevent an efficient lysosomal degradation. However, as the hydrophobic compartment of the hyperstar is small compared to common nanoparticle systems a translocation of the drug to hydrophobic domains within cellular compartments is more likely. The issue could be addressed in the future by including responsive building blocks to the polymer to introduce a stimuli responsive drug release.

Experimental part

Materials and Instrumentation

Propargyl alcohol, 3,3- dithiodipropionic acid, dithiothreitol (DTT), 4-(dimethylamino)- pyridine (DMAP), and 2,2-dimethoxy-2-phenylacetophenone (DMPA) were all purchased from Sigma-Aldrich. 1-Ethyl-3-(3-(dimethylamino)propyl)carbodiimide hydrochloride (EDC·HCl) was purchased from Iris Biotech. Triethylamine was purchased from Fischer Scientific. Triallyl 1,3,5-benzenetricarboxylate was purchased from Acros. All other materials were purchased from Fisher Scientific, Sigma-Aldrich, Merck, Fluka, and Acros. 2-Ethyl-2-oxazoline (EtOx) and methyl tosylate (MeTos) were distilled to dryness prior to use. EtOx was dried using CaH before distillation.

^{1}H-NMR spectra were measured using a Bruker DPX-300 or DPX-400 NMR spectrometer which operated at 300.13 and 400.05 MHz, respectively. The residual solvent peaks were used as internal references. Deuterated chloroform ($CDCl_3$) (δH = 7.26 ppm) was used as solvent for all measurements.

SEC measurements were performed on an Agilent 390-LC MDS instrument equipped with differential refractive index (DRI), viscometry (VS), dual angle light scatter (LS) and dual wavelength UV detectors. The system was equipped with 2 x PLgel Mixed D columns (300 x 7.5 mm) and a PLgel 5 µm guard column. The eluent is DMF with 5 mmol NH_4BF_4 additive. Samples were run at 1 ml/min at 50˚C. Poly(methyl methacrylate) standards (Agilent EasyVials) were used for calibration.

For SEC measurements in chloroform, an Agilent 390-LC MDS instrument with differential refractive index (DRI), viscometry (VS), dual angle light scatter (LS) and two wavelength UV detectors. The system was equipped with 2 x PLgel Mixed D columns (300 x 7.5 mm) and a PLgel 5 µm guard column. The eluent is $CHCl_3$ with 2 % TEA (triethylamine) additive. Samples were run at 1 mL min^{-1} at 30 °C. Poly(methyl meth-acrylate), and polystyrene standards (Agilent Easy Vials) were used for calibration.

Analyte samples were filtered through a nylon membrane with 0.22 µm pore size before injection. Respectively, experimental molar mass (Mn, SEC) and dispersity (Đ) values of synthesized polymers were determined by conventional calibration using Agilent GPC/SEC software.

Electrospray Ionisation (ESI) measurements were obtained using a Bruker MicroToF and the results analysed using Bruker Data Analysis. Samples were dissolved in methanol at a concentration of 1 µg mL^{-1}.

AFM pictures were taken on an Asylum Research MFP-3D Stand Alone atomic force microscope with extended z-range of 40 µm, with closed loop scanning in x and y over a range of 90 µm. Tapping mode was used for all measurements.

Di(prop-2-yn-1-yl) 3,3'-disulfanediyldipropionate (1)

3,3-dithiodipropionic acid (10.0 g, 47.56 mmol), N-(3-Dimethylaminopropyl)-N'-ethylcarbodiimide hydrochloride (EDC HCl) (21.88 g, 114.14 mmol) and 4-Dimethylaminopyridine (DMAP) (1.14 g, 9.52 mmol) were added to a round bottom flask containing 250 mL of dimethylformamide (DMF) cooled in an ice bath and left to stir. Propargyl alcohol (6.4 g, 114.14 mmol) was slowly added to the solution and the RBF removed from the ice bath and allowed to reach room temperature before leaving to stir for 70 hr. The DMF was removed and the concentrated product was re-dissolved in DCM (250 mL). The DCM phase was then washed with water (3 x 100 mL) followed by washes with HCl (1 x 100 mL), NaOH (1 x 100 mL) and water (1 x 100 mL) before drying over Na_2SO_4. DCM was removed by rotary evaporation and the product purified by column chromatography to yield a yellow-orange oil, di(prop-2-yn-1-yl) 3,3'-disulfanediyldipropionate (9.8 g, 34.2 mmol, 72.1 %).

^{1}H NMR (400 MHz, $CDCl_3$) δ ppm: 4.74 (s, 2H, O−CH_2≡C), 2.97 (t, 2H, C(O)−CH_2−CH_2), 2.82 (t, 2H, CH_2−CH_2−S), 2.51 (s, 1H, C≡CH). ^{13}C NMR (100 MHz, $CDCl_3$) δ ppm: 170.91 (C=O), 76.84 (CH_2−C≡CH), 75.25 (C≡CH), 52.32 (O−CH_2−C≡), 33.86 (C(O)−CH_2−CH_2), 32.79 (CH_2−CH_2−S).

Prop-2-yn-1-yl 3-mercaptopropanoate (2)

Di(prop-2-yn-1-yl) 3,3'-disulfanediyldipropionate (0.5 g, 1.75 mmol) was dissolved in dichloromethane (DCM) (7 mL) before addition of dithiothreitol (DTT) (1.17 g, 7.66 mmol) and trimethylamine (1.12 mL, 8.00 mmol). The solution was deoxygenated by purging with nitrogen for 10 minutes before being left to stir at room temperature for 2 hr. The solution was then washed with HCl (1 x 10 mL) and water (1 x 10 mL) and then dried over Na_2SO_4 and the solvent removed resulting in a yellow oil, prop-2-yn-1-yl 3-mercaptopropanoate (0.14 g, 0.97 mmol, 28 %), that was stored under nitrogen to prevent formation of disulfides.

^{1}H NMR (400 MHz, $CDCl_3$) δ ppm: 4.71 (s, 2H, O−CH_2−C≡), 2.79 (m, 2H, C(O)−CH_2−CH_2), 2.71 (m, 2H, CH_2−CH_2−SH), 2.49 (s, 1H, C≡CH), 1.66 (t, 1H, CH_2−SH). ^{13}C NMR (100 MHz, $CDCl_3$) δ ppm: 170.81 (C=O), 76.84 (CH_2−C≡CH), 75.20 (C≡CH), 52.15 (O−CH_2−C≡), 38.16 (C(O)−CH_2−CH_2), 19.56 (CH_2−CH_2−SH).

Preparation of branch-poly(prop-2-yn-1-yl 3-mercaptopropanoate) (3)

Prop-2-yn-1-yl 3-mercaptopropanoate (100 mg, 0.69 mmol) and 2,2-dimethoxy-2-phenylacetophenone (DMPA) (2 mg, 16.7 µmol) were dissolved in dimethylformamide (DMF) (318 µL). The solution was deoxygenated by nitrogen purging and added to a 250 µL Hamilton Gastight glass syringe with stainless steel cannula and wrapped in aluminium foil. In a second vial, 1,3,5-Benzenetricarboxylic acid triallyl ester (11.46 mg, 34.7 µmol) and DMPA (1 mg, 8.4 µmol) were dissolved in DMF and deoxygenated by nitrogen bubbling. The Hamilton syringe was placed into an automated pump and the needle fed into the second vial containing the core, which was then placed in an aluminium foil lined box and covered with a 365 nm UV lamp (UVP, UVGL-55, 6 watt). The monomer was then fed into the vial at a rate of 10.45 µL min^{-1}. After the feeding finished the needle was removed and the vial was left under UV light for a further 1 hour. The solution was then precipitated into diethyl ether and centrifuged to separate the polymer from solvent. The diethyl ether was decanted and the polymer dried with nitrogen to remove any residual solvent. A stock solution of the hyperbranched core in dimethylformamide (20 mg mL^{-1}) was prepared and stored in a freezer.

SEC (DMF, NH_4BF_4): Mn = 6,000 g mol^{-1}, $Đ$ = 1.29;

Kinetic study of poly(oxazoline) polymerisation

Dry ethyl oxazoline (EtOx), methyl tosylate (MeTos) and acetonitrile were added to a schlenk flask under nitrogen and left to stir in an oil bath at 80 °C. At pre-determined time intervals, aliquots of the reaction mixture were removed using a pre heated needle and analysed by SEC and NMR spectroscopy. Conversions, as well as SEC data are presented in **Table 3**.

Table 3: Analytical data of PEtOX kinetic samples.

Time (min)	Conversion (%)	$M_{n,\,SEC}$ (g mol^{-1})	$Đ$
10	4.3	500	1.04
30	9.1	700	1.12
60	28.0	1,200	1.17
120	61.5	2,000	1.17
180	76.0	2,400	1.22
240	93.1	3,000	1.09
300	93.9	2,700	1.24

Preparation of Xanthate terminated Poly(oxazoline)s (4, 5)

Dry ethyl oxazoline (EtOx), methyl tosylate (MeTos) and acetonitrile (**Table 4**) were added to a Schlenk flask under nitrogen and left to stir in an oil bath at 80 °C. After a predetermined time, the solution was removed from the oil bath, a sample for determination of the conversion was taken, and potassium ethyl xanthate was added to terminate the polymer chain. The product was left to stir for 1 hr before being diluted with chloroform (100 mL). The organic layer was then washed with sat. Na_2CO_3 (3 x 100 mL) and brine (3 x 100 mL) then dried over $MgSO_4$. The chloroform was removed to leave a colourless oil. The oil was re-dissolved in DCM (10 mL) and precipitated into ether and the polymer collected by gravity filtration as a white solid. The white solid was again re-dissolved into DCM which was evaporated. Subsequently, the polymer was dried under vacuum to yield a white solid.

Table 4: Composition of the reactions mixtures for the synthesis of xanthate end functionalized PEtOx.

Sample	Target DP	EtOx (mL)	MeTos (mL)	Acetonitrile (mL)	Ethyl Xanthate (mg)	Time (min)
4	25	4.058	0.243	7.699	309	186
5	50	4.038	0.121	5.841	462	311

^{1}H NMR (5, 300 MHz, $CDCl_3$) δ ppm: 3.75 – 3.13 (m, 168 H, backbone), 3,10 - 2.92 (m, 3 H, Methyl group (α-end)), 2.54 - 2.13 (m, 87 H, CH_2 side chain), 1.44 (t, 2.7 H, Methyl group (xanthate)), 1.23 – 0.98 (m, 124 H, CH_3 side chain);

SEC ($CHCl_3$, trimethylamine, PS calibration): Mn = 5,900 g mol^{-1}, $Đ$ = 1.12;

ESI-ToF (4): measured: 1843.039 m/z ($M+K^+$), simulated: 1843.130 m/z;

Preparation of PEtOx-S-S-PEtOx (6, 7)

PEtOx-xanthate (1.4 g, 53.8 mmol) was dissolved in diethylamine (33% in EtOH) (20 mL) and stirred at 40°C for 3 hr. The reaction mixture was then poured over a solution of sulphuric acid (H_2SO_4) (20 mL) and ice-water (200 mL). The polymer was extracted by washing with $CHCl_3$ (3 x 50 mL), followed by washing of the $CHCl_3$ layer with sat. Na_2CO_3 (3 x 100 mL) and brine (3 x 100 mL). The organic layer was then dried over $MgSO_4$ and filtered before the solvent removed to yield disulfide-poly(oxazoline).

^{1}H NMR (7, 300 MHz, $CDCl_3$) δ ppm: 3.75 – 3.13 (m, 166 H, backbone), 3,10 - 2.92 (m, 3 H, Methyl group (α-end)), 2.54 - 2.13 (m, 88 H, CH_2 side chain, 1.23 – 0.98 (m, 123 H, CH_3 side chain);

SEC ($CHCl_3$, trimethylamine, PS calibration): Mn = 11,700 g mol^{-1}, $Đ$ = 1.11;

Preparation of thiol-terminated poly(oxazoline) (8, 9)

Disulfide-poly(oxazoline) (130 mg, 26.3 µmol) was dissolved in DCM (5 mL) before addition of DTT (17.8 mg, 115.7 µmol) and triethylamine (16.8 µL, 120.9 µmol). The solution was deoxygenated by purging with N_2 for 10 minutes, before being left to stir for 2 hr. The solution was then washed with deoxygenated HCl (1 x 10 mL), sat. Na_2CO_3 (1 x 10 mL) and brine (1 x 10 mL) and then dried over Na_2SO_4 and the solvent removed, yielding the thiol terminated poly(oxazoline). The polymer was stored under N_2 to prevent oxidation of the thiol back to disulfide.

ESI-ToF (4): measured: 2151.313 m/z ($M+K^+$), simulated: 2151.424 m/z;

Preparation of branch-poly(prop-2-yn-1-yl 3-mercaptopropanoate)-star-poly(oxazoline) (10, 11)

A stock solution of poly(oxazoline) in DMF (200 mg/mL) was prepared and added to the hyperbranched core stock solution (20 mg mL^{-1}) at a 0.66:1 ratio of poly(oxazoline):alkyne groups. DMPA was added (**Table 5**) and the resulting solution deoxygenated, by N_2 purging, for 10 minutes before being placed under a 365 nm UV lamp (UVP, UVGL-55, 6 watt) for 24 hr. The solution was then precipitated into diethyl ether and the resulting precipitate recovered before being redissolved in DMF and precipitated into water to remove any residual hyperbranched core. The excess poly(oxazoline) was removed by using an appropriately sized centrifuge membrane filter (10 kDa MWCO for DP 25 POx, 30 KDa MWCO for DP 50). The solution was passed through the membrane 5 times to ensure complete removal of the poly(oxazoline) and then placed on the freeze-dryer over night to remove the water and leave the resulting hyperstar polymer.

SEC (10, DMF, NH_4BF_4): Mn = 13,800 g mol^{-1}, $Đ$ = 1.30;

Table 5: Composition of reaction mixtures for the synthesis of hyperstar copolymers.

Sample	Poly(PYMP) (mg)	PEtOx (mg)	DMPA (mg)	DMF (mL)
10	48.8	300	19.7	3.94
11	22.8	280	12.7	2.54

Static light scattering

The incremental refractive index, d*n*/d*C*, was determined by measuring the refractive index of the polymer over a range of concentrations. The RI was determined using a Shodex RI detector, operating at a wavelength of 632 nm. Multiplying the gradient, of the plot of RI vs conc., by the refractive index of the solvent (water = 1.3325) and dividing by the RI constant of the instrument (-1,398,000) gives the d*n*/d*C* of the polymer.

Table 6: Incremental refractive indices of poly(PYMP) and hyperstar copolymers.

Sample	dn/dC in water	dn/dC in DMF
3	-	0.102
10	0.17	0.093
11	0.16	0.101

Light scattering measurements were obtained using an ALV-CGS3 system operating with a vertically polarized laser with wavelength λ = 632 nm. The measurements were taken at 20 °C over a range of scattering wave vectors ($q = 4\pi n \sin(\theta/2)/\lambda$, with θ the angle of observation and n the refractive index of the solvent). The Rayleigh ratio, R_θ, was determined using eq. 1,

$$R_\theta = \frac{I_{solution}(\theta) - I_{solvent}(\theta)}{I_{toluene}(\theta)} \cdot \left(\frac{n_{solvent}}{n_{toluene}}\right)^2 \cdot R_{toluene} \quad (1)$$

where $I_{solution}$, $I_{solvent}$ and $I_{toluene}$ are the scattering intensities of the solution, solvent and reference (toluene) respectively, n is the refractive index (n_{water} = 1.333, n_{dmf} = 1.431, $n_{toluene}$ = 1.496) and $R_{toluene}$ the Rayleigh ratio of toluene ($R_{toluene}$ = 1.35 x 10^{-5} cm^{-1} for λ = 632.8 nm).

The optical constant, K, is defined by eq. 2, where N_a is Avogadro number and dn/dC is the incremental refractive index.

$$K = \frac{4\pi^2 n_{solvent}^2}{\lambda^4 N_a}\left(\frac{\partial n}{\partial C}\right)^2 \quad (2)$$

In all cases it was verified that the apparent radius of gyration of the systems verified $q \times R_g < 1$. The Zimm approximation can thus be used to obtain eq. 3. Plotting KC/Rθ as a function of q^2 for each concentration yielded the apparent radius of gyration Rg of the scatterers as well as their apparent molecular weight extrapolated to zero angle, Ma. Representative plots are shown in the Supporting Information.

$$\frac{KC}{R_\theta} = \frac{1}{M_a} \cdot \left(1 + \frac{q^2 \cdot R_g^2}{3}\right) \quad (3)$$

At a given concentration the Rayleigh ratio, R_θ, is related to the apparent molecular weight of the sample, given by eq. 3. It is only at infinite dilutions, where the interactions between scattering particles are negligible, that the apparent molecular weight is equal to the true molecular weight.[55] Multiple concentrations were measured and a plot of linear regression used to determine the apparent molecular weight at a concentration of 0 mg mL^{-1}.

Fluorescence and Absorbance measurements

Fluorescence spectra were measured using a Cary Eclipse Fluorescence Spectrophotometer from Agilent. Samples were excited at a wavelength of 520 nm and the fluorescence intensity was recorded between 530 and 700 nm in 2 nm intervals. Absorbance spectra were obtained using a Cary 60 UV-Vis spectrometer from Agilent.

To probe nile red uptake of hyperstars nile red was dissolved in THF at a concentration of 0.796 mg mL^{-1}. 40 µL of that solution (100 nmol) were added to a vial containing hyperstar in THF (1.96 mL) resulting in a final nile red concentration of 50 µmol L^{-1}. The concentration of hyperstar was varied starting with an overall concentration of 1 mg mL^{-1}. Different concentrations were obtained performing a serial 2 fold dilution. The THF was left to evaporate under ambient conditions over 24 h. Subsequently, water (2 mL) was added to each vial and stirred for 2 h to solubilize hyperstar copolymers. The water was filtered using 0.2 µm syringe filters and 1.5 mL were freeze dried. The resulting solid was dissolved in THF and absorbance as well as fluorescence was recorded.

Nile red calibration was performed using a 50 µmol L^{-1} solution of the dye in THF and a 2 fold serial dilution approach. The intensity was determined at 520 nm.

Cell Culture

A2780 human ovarian carcinoma cells were used between passages 5 and 25 and grown in Roswell Park Memorial Institute medium (RPMI-1640) supplemented with 10% of fetal

calf serum, 1% of 2 mM glutamine and 1% penicillin/streptomycin. The cells were grown as adherent monolayers at 310 K in a 5% CO_2 humidified atmosphere and passaged at approximately 70-80% confluence.

In vitro growth inhibition assays

The antiproliferative activity of polymers 10 and 11 was determined in A2780 ovarian cancer cells. Briefly, 96-well plates were used to seed 5000 cells per well. The plates were left to pre-incubate with drug-free medium at 310 K for 24 h before adding different concentrations of the compounds to be tested (2 mg ml^{-1}-200 ng ml^{-1}). A drug exposure period of 72 h was allowed. The SRB assay was used to determine cell viability. GI_{50} values, as the concentration which causes 50% cell death, were determined as duplicates of triplicates in two independent sets of experiments and their standard deviations were calculated.

Confocal microscopy

A2780 ovarian carcinoma cells were seeded in 8-well microscopy chambers (15000 cells/well; 200 µl phenol red free DMEM medium), left to attach for 24 h, and then treated for another 2 h with 0.1 mg/ml of the hyperbranched polymers loaded with Nile Red (λ_{ex} = 520 nm/λ_{em} = 590 nm). Cell nuclei were stained using Hoechst 33258 (2.5 µg/ml; 30 min at 37C; λ_{ex} = 352 nm/λ_{em} = 461 nm), and either lysosomes or mitochondria were labelled with LysoTracker® Green DND-26 (50 nM; 30 min at 37C; λ_{ex} = 504 nm/λ_{em} = 511 nm) or MitoTracker® Green FM (400 nM; 30 min at 37C; λ_{ex} = 490 nm/λ_{em} = 516 nm), respectively. Cells were then washed with PBS and fresh phenol red free medium added. Cells where then imaged using a Leica SP5 or a Zeiss LSM 880 confocal microscope. Images were open and processed using FIJI ImageJ package.

Conclusion & Outlook

In summary, we were able to produce well-defined hyperstar copolymers by the combination of thiol-yne and POx chemistries. The core was based on narrow dispersity (1.29) thiol-yne hyperbranched polymer with a high degree of branching (0.9), and the shell produced from water soluble Poly(2-Ethyl-2-oxazoline) (PEtOx) chains bearing thiol end groups. In order to study the influence of the hydrophilic shell on the properties of the resulting hyperstar, the DP of the PEtOx was varied. The thiol end group was generated from a xanthate moiety, which was used to terminate the living polymerization of EtOx. Conjugation was performed using a radical based thiol-yne addition process.

Hyperstar copolymers were characterized using SEC, NMR spectroscopy and SLS in order to assess structural information. Minor aggregation was found to be present in DMF as well as in water for PEtOx shells with DP 25 and 50 likewise, which was ascribed to the presence of remaining hydrophobic patches on the hyperstar as well as to entanglement during purification. For both DPs of PEtOx the number of arms per hyperbranched core was around 20. The encapsulation of nile red into the hyperbranched core of the polymers was studied and found to be dependent on the nature of the shell with values between 1 and 2 mol%.

In order to evaluate the potential of the produced polymers as drug delivery vectors, cytotoxicity was assessed using A2780 human ovarian carcinoma cells. IC_{50} values were found to be around 0.7 mg mL^{-1} regardless of the length of the PEtOx constituting the shell. This concentration is well above the dose of polymer used in a drug delivery application. Hyperstars were found to be internalized into cells and colocalized within lysosomal compartments.

Future studies will focus on the implementation of cleavable units within the hyperbranched core, able to trigger a release, as well as on further functionalization of the system using residual alkynes or alkenes.

Acknowledgements

MH gratefully acknowledges the German Research Foundation (DFG, GZ: HA 7725/1-1) for funding. The Royal Society Wolfson Merit Award (WM130055; S.P.), Monash-Warwick Alliance (S.P.), and Syngenta (A.C.) are acknowledged for financial support. CSC gratefully acknowledges Cancer Research UK (C53561/A19933).

References

1. T. L. Doane and C. Burda, *Chem. Soc. Rev.*, 2012, **41**, 2885-2911.
2. M. E. Davis, Z. Chen and D. M. Shin, *Nat. Rev. Drug Discov.*, 2008, **7**, 771-782.
3. H. Cabral and K. Kataoka, *J. Control. Release*, 2014, **190**, 465-476.
4. H. Maeda, K. Greish and J. Fang, in *Polymer Therapeutics II*, eds. R. Satchi-Fainaro and R. Duncan, Springer Berlin Heidelberg, 2006, vol. 193, ch. 26, pp. 103-121.
5. L. Dai, J. Liu, Z. Luo, M. Li and K. Cai, *J. Mater. Chem. B*, 2016, **4**, 6758-6772.
6. V. P. Torchilin, *J. Control. Release*, 2001, **73**, 137-172.
7. P. Kesharwani, K. Jain and N. K. Jain, *Prog. Polym. Sci.*, 2014, **39**, 268-307.
8. C. Gao and D. Yan, *Prog. Polym. Sci.*, 2004, **29**, 183-275.
9. E. Malmstroem, M. Johansson and A. Hult, *Macromolecules*, 1995, **28**, 1698-1703.
10. D. Konkolewicz, A. Gray-Weale and S. Perrier, *J. Am. Chem. Soc.*, 2009, **131**, 18075-18077.
11. Y. Shi, R. W. Graff, X. Cao, X. Wang and H. Gao, *Angew. Chem. Int. Ed.*, 2015, **54**, 7631-7635.
12. L. Zou, Y. Shi, X. Cao, W. Gan, X. Wang, R. W. Graff, D. Hu and H. Gao, *Polymer Chemistry*, 2016, **7**, 5512-5517.
13. C. Gao, D. Yan and H. Frey, in *Hyperbranched Polymers*, John Wiley & Sons, Inc., 2011, DOI: 10.1002/9780470929001.ch1, pp. 1-26.
14. A. B. Cook, R. Barbey, J. A. Burns and S. Perrier, *Macromolecules*, 2016, **49**, 1296-1304.
15. M. C. Lukowiak, B. N. S. Thota and R. Haag, *Biotechnol. Adv.*, 2015, **33**, 1327-1341.

16. J. Kronek, Z. Kroneková, J. Lustoň, E. Paulovičová, L. Paulovičová and B. Mendrek, *J. Mater. Sci. Mater. Med.*, 2011, **22**, 1725-1734.
17. J. Kronek, E. Paulovičová, L. Paulovičová, Z. Kroneková and J. Lustoň, *J. Mater. Sci. Mater. Med.*, 2012, **23**, 1457-1464.
18. R. Luxenhofer, G. Sahay, A. Schulz, D. Alakhova, T. K. Bronich, R. Jordan and A. V. Kabanov, *J. Control. Release*, 2011, **153**, 73-82.
19. M. C. Woodle, C. M. Engbers and S. Zalipsky, *Bioconjugate Chem.*, 1994, **5**, 493-496.
20. S. Zalipsky, C. B. Hansen, J. M. Oaks and T. M. Allen, *J. Pharm. Sci.*, 1996, **85**, 133-137.
21. M. Platen, E. Mathieu, S. Lück, R. Schubel, R. Jordan and S. Pautot, *Biomacromolecules*, 2015, **16**, 1516-1524.
22. L. Wyffels, T. Verbrugghen, B. D. Monnery, M. Glassner, S. Stroobants, R. Hoogenboom and S. Staelens, *J. Control. Release*, 2016, **235**, 63-71.
23. B. Guillerm, S. Monge, V. Lapinte and J.-J. Robin, *Macromol. Rapid Commun.*, 2012, **33**, 6000-6016.
24. K. Lava, B. Verbraeken and R. Hoogenboom, *Eur. Polym. J.*, 2015, **65**, 98-111.
25. M. N. Leiske, M. Hartlieb, C. Paulenz, D. Pretzel, M. Hentschel, C. Englert, M. Gottschaldt and U. S. Schubert, *Adv. Funct. Mater.*, 2015, **25**, 2458-2466.
26. Z. He, X. Wan, A. Schulz, H. Bludau, M. A. Dobrovolskaia, S. T. Stern, S. A. Montgomery, H. Yuan, Z. Li, D. Alakhova, M. Sokolsky, D. B. Darr, C. M. Perou, R. Jordan, R. Luxenhofer and A. V. Kabanov, *Biomaterials*, 2016, **101**, 296-309.
27. J. Li, Y. Zhou, C. Li, D. Wang, Y. Gao, C. Zhang, L. Zhao, Y. Li, Y. Liu and X. Li, *Bioconjugate Chem.*, 2015, **26**, 110-119.
28. K. Knop, D. Pretzel, A. Urbanek, T. Rudolph, D. H. Scharf, A. Schallon, M. Wagner, S. Schubert, M. Kiehntopf, A. A. Brakhage, F. H. Schacher and U. S. Schubert, *Biomacromolecules*, 2013, **14**, 2536-2548.
29. S. Lück, R. Schubel, J. Rüb, D. Hahn, E. Mathieu, H. Zimmermann, D. Scharnweber, C. Werner, S. Pautot and R. Jordan, *Biomaterials*, 2016, **79**, 1-14.
30. M. Hartlieb, D. Pretzel, M. Wagner, S. Hoeppener, P. Bellstedt, M. Gorlach, C. Englert, K. Kempe and U. S. Schubert, *J. Mater. Chem. B*, 2015, **3**, 1748-1759.
31. C. Legros, A.-L. Wirotius, M.-C. De Pauw-Gillet, K. C. Tam, D. Taton and S. Lecommandoux, *Biomacromolecules*, 2015, **16**, 183-191.
32. V. M. Gaspar, P. Baril, E. C. Costa, D. de Melo-Diogo, F. Foucher, J. A. Queiroz, F. Sousa, C. Pichon and I. J. Correia, *J. Control. Release*, 2015, **213**, 175-191.
33. K. Kempe, S. L. Ng, S. T. Gunawan, K. F. Noi and F. Caruso, *Adv. Funct. Mater.*, 2014, **24**, 6187-6194.
34. S. T. Gunawan, K. Kempe, T. Bonnard, J. Cui, K. Alt, L. S. Law, X. Wang, E. Westein, G. K. Such, K. Peter, C. E. Hagemeyer and F. Caruso, *Adv. Mater.*, 2015, **27**, 5153-5157.
35. M. Hartlieb, K. Kempe and U. S. Schubert, *J. Mater. Chem. B*, 2015, **3**, 526-538.
36. P. Wilson, P. Chun Ke, T. P. Davis and K. Kempe, *Eur. Polym. J.*, DOI: http://dx.doi.org/10.1016/j.eurpolymj.2016.09.011.
37. A. Kowalczuk, J. Kronek, K. Bosowska, B. Trzebicka and A. Dworak, *Polym. Int.*, 2011, **60**, 1001-1009.
38. F. Däbritz, A. Lederer, H. Komber and B. Voit, *J. Polym. Sci., Part A: Polym. Chem.*, 2012, **50**, 1979-1990.
39. R. Weberskirch, R. Hettich, O. Nuyken, D. Schmaljohann and B. Voit, *Macromol. Chem. Phys.*, 1999, **200**, 863-873.
40. A. Pospisilova, S. K. Filippov, A. Bogomolova, S. Turner, O. Sedlacek, N. Matushkin, Z. Cernochova, P. Stepanek and M. Hruby, *RSC Advances*, 2014, **4**, 61580-61588.
41. H. M. L. Lambermont-Thijs, M. W. M. Fijten, U. S. Schubert and R. Hoogenboom, *Aust. J. Chem.*, 2011, **64**, 1026-1032.
42. R. B. Restani, J. Conde, R. F. Pires, P. Martins, A. R. Fernandes, P. V. Baptista, V. D. B. Bonifácio and A. Aguiar-Ricardo, *Macromol. Biosci.*, 2015, **15**, 1045-1051.
43. C. Zhang, S. Liu, L. Tan, H. Zhu and Y. Wang, *J. Mater. Chem. B*, 2015, **3**, 5615-5628.
44. S. Park Yong, S. Kang Yong and J. Chung Dong, *Journal*, 2002, **2**, 211.
45. R. M. England, J. I. Hare, P. D. Kemmitt, K. E. Treacher, M. J. Waring, S. T. Barry, C. Alexander and M. Ashford, *Polym. Chem.*, 2016, **7**, 4609-4617.
46. R. M. England, J. I. Hare, J. Barnes, J. Wilson, A. Smith, N. Strittmatter, P. D. Kemmitt, M. J. Waring, S. T. Barry, C. Alexander and M. B. Ashford, *J. Control. Release*, 2017, **247**, 73-85.
47. Y. Shimano, K. Sato and S. Kobayashi, *J. Polym. Sci., Part A: Polym. Chem.*, 1995, **33**, 2715-2723.
48. O. Koshkina, D. Westmeier, T. Lang, C. Bantz, A. Hahlbrock, C. Würth, U. Resch-Genger, U. Braun, R. Thiermann, C. Weise, M. Eravci, B. Mohr, H. Schlaad, R. H. Stauber, D. Docter, A. Bertin and M. Maskos, *Macromol. Biosci.*, 2016, **16**, 1616-5195.
49. G.-H. Hsiue, H.-Z. Chiang, C.-H. Wang and T.-M. Juang, *Bioconjugate Chem.*, 2006, **17**, 781-786.
50. V. R. de la Rosa, Z. Zhang, B. G. De Geest and R. Hoogenboom, *Adv. Funct. Mater.*, 2015, **25**, 2511-2519.
51. M. Le Neindre, B. Magny and R. Nicolay, *Polym. Chem.*, 2013, **4**, 5577-5584.
52. C. S. Popeney, M. C. Lukowiak, C. Böttcher, B. Schade, P. Welker, D. Mangoldt, G. Gunkel, Z. Guan and R. Haag, *ACS Macro Letters*, 2012, **1**, 564-567.
53. E. Burakowska and R. Haag, *Macromolecules*, 2009, **42**, 5545-5550.
54. G. Chen and Z. Guan, *J. Am. Chem. Soc.*, 2004, **126**, 2662-2663.
55. W. Brown, *Light Scattering: Principles and Development*, Clarendon Press, 1996.